Transport of airborne particles in straight and curved microchannels

Document Version:
Publisher's PDF, also known as Version of Record (includes final page, issue and volume numbers)

Please check the document version of this publication:

• A submitted manuscript is the version of the article upon submission and before peer-review. There can be important differences between the submitted version and the official published version of record. People interested in the research are advised to contact the author for the final version of the publication, or visit the DOI to the publisher's website.
• The final author version and the galley proof are versions of the publication after peer review.
• The final published version features the final layout of the paper including the volume, issue and page numbers.

[Link to publication](#)

Transport of airborne particles in straight and curved microchannels

Allison Schaap,[1] Winnie C. Chu,[2] and Boris Stoeber[1,3]

[1]*Department of Mechanical Engineering, The University of British Columbia, Vancouver V6T 1Z4, Canada*
[2]*School of Environmental Health, The University of British Columbia, Vancouver V6T 1Z3, Canada*
[3]*Department of Electrical and Computer Engineering, The University of British Columbia, Vancouver V6T 1Z4, Canada*

The measurement of airborne particles is important for environmental and exposure monitoring. Microfluidic technologies present potential advantages for aerosol monitoring but have been applied very little to the handling of airborne particles. In this paper, we examine the flow focusing and cross-streamline diffusion of aerosols in straight microchannels, and the size-based lateral displacement of aerosols caused by centrifugal forces in a curved channel. We present calculations, simulations, and experimental results verifying the models: measurements of the focusing and diffusion of 0.2 μm and 0.75 μm particles in straight channels and of the size-dependent lateral displacement of particles between 0.2 μm and 2 μm in curved channels are demonstrated and shown to match well with the simulations. We observe lateral dispersion of the particles: particles closer to the top and bottom wall of the channel experience less lateral displacement than particles near the center due to the flow velocity distribution across the channel cross section. These results confirm that the microchannel techniques presented are a viable method for the size-based manipulation of airborne particles. © *2012 American Institute of Physics.* [http://dx.doi.org/10.1063/1.4742900]

I. INTRODUCTION

Microfluidics research and development has emerged as a novel and promising tool for the development of applications as varied as cell sorting,[1,2] chemical and biochemical analysis,[3] drug discovery,[4] chemical reactors,[5] and others.[6,7] These applications have been coupled with the parallel development of appropriate liquid handling tools such as micropumps[8] and valves[9] as well as the study of the fluid mechanics of such devices.[10,11] However, one area in which microfluidics has been only minimally employed is in the handling of airborne particles or aerosols. Aerosols with diameters of less than half a micrometer have been sorted by size in microchannels using electrostatic forces,[12] and a micromachined virtual impactor was used to sort aerosols into two size bins with a fixed cutoff diameter around 1 μm.[13] Mass-measurements of particulate matter deposited onto thin-film bulk acoustic wave resonators[14] and thermally actuated silicon resonators[15] have also been presented. These approaches demonstrated high resolution and sensitivity to low concentration levels but do not inherently include a size-selective mechanism that would allow the device to characterize the concentration of particular sizes of aerosol.

Exposure to aerosols through inhalation has been shown to negatively affect human health and has been linked to increased rates of asthma, cardiovascular disease, lung cancer, pulmonary diseases, and mortality.[16–18] As a result of these effects, occupational and health regulatory agencies worldwide have set limits on the recommended levels of environmental aerosols as well as occupational exposure limits. The small size of microchannels coupled with the opportunity to integrate sensing technologies suggests them as a promising tool for the next generation of aerosol sensors.
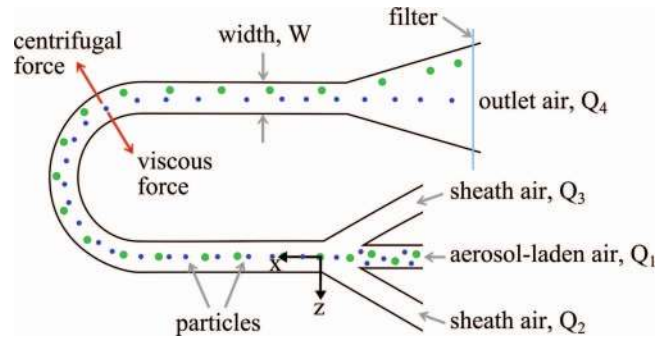
24, 083301-1

FIG. 1. Principle of operation of curved microchannel with centrifugal-force-based size-specific displacement of airborne particles.

In general, one of the most sought-after advantages of microfluidics is the potential to take advantage of low-cost bulk fabrication processes, generally characterized by the small size of achievable device features and high level of on-chip integration. A microfluidics chip approach to aerosol handling and monitoring is a potentially potent tool for monitoring personal exposure to aerosols or high-resolution spatial monitoring of particulate matter levels. Towards that end, we investigate the transport of aerosols in microchannels with a focus on modeling and measuring the effects of aerodynamic focusing, particle diffusion, and the centrifugal forces acting on particles in a curved microchannel leading to lateral displacement (Figure 1). Each of these effects is described, simulated, and then measured to finally demonstrate the size-dependent lateral movement of airborne particles in a curved microchannel including the effect of lateral dispersion.

II. THEORY

We confine particles to a region in the center of the channel with sheath air. The ability to focus the stream of particles directly relates to the intended eventual application of the device; namely, the size-separation of particles by centrifugal forces. The effect of the focusing is counteracted by the diffusion of the particles out of the focused aerosol stream. The descriptions of these three effects – flow focusing, diffusion, and the size-specific motion of particles from centrifugal force – are developed here.

A. Width of particle-laden stream

The characteristically small dimensions of microchannels typically lead to flows with low Reynolds numbers

$$Re = \frac{\rho V D_H}{\mu},\tag{1}$$

with the hydraulic diameter $D_H = 2WH/(W+H)$ of a rectangular channel of width W and height H and a fluid of density ρ, velocity V, and viscosity μ. In the case of low Reynolds numbers, the inertial terms of the Navier-Stokes equations can be neglected, leading to the equation of unidirectional flow

$$\frac{\partial^2 V}{\partial y^2} + \frac{\partial^2 V}{\partial z^2} = \frac{1}{\mu}\frac{dp}{dx},\tag{2}$$

with V in the x-direction along the channel and with the pressure gradient dp/dx. With the no-slip condition imposed on the walls, (2) yields the flow profile

$$V(y,z) = \frac{4H^2}{\mu\pi^3}\frac{P_0}{L}\sum_{n_{odd}}^{\infty}(-1)^{\frac{n-1}{2}}\left\{1 - \frac{\cosh\left[\frac{n\pi z}{H}\right]}{\cosh\left[\frac{n\pi W}{H}\right]}\right\}\frac{\cos\left[\frac{n\pi y}{H}\right]}{n^3}\tag{3}$$

for $-H/2 < y < H/2$ and $-W/2 < z < W/2$ and with a total pressure drop P_0 along the channel of length L.[19]

The flow resistance R is defined as the total pressure drop along the channel divided by the flow rate Q through the channel. For a rectangular channel, the resistance per length,

$$\frac{R}{L} = \frac{P_0}{QL} = \frac{12\mu}{H^3 W} \times \left[1 - \frac{192H}{\pi^5 W} \sum_{n_{odd}}^{\infty} \left\{ \frac{\tanh\left(\frac{n\pi W}{2H}\right)}{n^5} \right\} \right]^{-1}, \tag{4}$$

is found by integrating the velocity profile (Eq. (3)) to find the total flow rate, dividing by the pressure drop, and inverting the equation.[19]

In the present work, the stream of air ($\mu = 1.8 \times 10^{-5}$ Pa s) containing particles was aerodynamically focused with two sheath air lines (Figure 1). The inlets for sheath air and particle-laden air were all pressure-controlled; the flow resistances of the individual sections were used to calculate the flow rates Q_i of the sheath air and aerosol stream as a function of the driving pressures P_i with a fluidic version of Ohm's Law.[19] Solving first for the pressure at the node (where the inlet channels merge to form the exit channel),

$$P_C = \left(\sum_{i=1}^{4} \frac{P_i}{R_i} \right) \times \left(\frac{R_1 R_2 R_3 R_4}{R_1 R_2 R_3 + R_1 R_2 R_4 + R_1 R_3 R_4 + R_2 R_3 R_4} \right), \tag{5}$$

provides the flow rates Q_i of each section, where R_1 is the flow resistance of the aerosol channel, R_2 and R_3 that of the sheath flow channels, and R_4 that of the main outlet channel plus any other fluidic resistances; for example, that of a filter collecting particles at the channel exit. This allows calculation of the width of the aerosol flow in the outlet by determining the width of each sheath air section z_o with

$$\frac{\int_0^{z_o} \int_0^h V(y, z)\, dy\, dz}{\int_0^w \int_0^h V(y, z)\, dy\, dz} = \frac{Q_s}{2Q_s + Q_1} \tag{6}$$

for $Q_S = Q_2 = Q_3$.

B. Diffusion of aerosol particles

The Brownian motion of air molecules affects the position of small airborne particles, resulting in a time-dependent stochastic diffusion process by which a region of concentrated particles will gradually spread out. As a result, Brownian motion will cause the stream of particles to gradually widen into the sheath air.

In two dimensions, the conditional probability

$$P(y, z, t) = \frac{1}{\sqrt{16\pi^2 Dt}} \exp\left[\frac{-(y^2 + z^2)}{8Dt} \right] \tag{7}$$

that a particle will be found at position (y,z) at time t is a normal distribution with a mean of zero and a standard deviation with the resulting RMS distance $\langle L_{2D} \rangle = \sqrt{4Dt}$. The translational diffusion coefficient

$$D = \frac{k_B T C_S}{3\pi\mu d} \tag{8}$$

of a particle of diameter d depends on the particle and fluid characteristics as well as on the Boltzmann constant k_B, the temperature T in Kelvin, and the Cunningham slip correction factor

$$C_S = 1 + \frac{2\lambda}{d} \left(A_1 + A_2 \exp\left(\frac{A_3 d}{\lambda} \right) \right), \tag{9}$$

which is a correction to the drag force predicted by the Stokes equations. The experimentally determined constants $A_1 = 1.257$, $A_2 = 0.40$, and $A_3 = 0.55$ correct for a sphere travelling through

air at standard temperature and pressure.[20] We describe the particle diffusion with the Péclet number,

$$Pe = \frac{L\bar{V}}{D},$$ (10)

based on the average flow velocity $\bar{V}$ along the curved channel and the length L along this channel until the detection region to express the relative effects of advection and diffusion.

C. Particle displacement due to centrifugal forces

To realize a size-specific motion of the particles, a curved microchannel was used to impart centrifugal forces on the test aerosols (Figure 1). For a sphere of density ρ, diameter d, and resulting mass m, moving in an arc of radius r with velocity V, the centrifugal force,

$$F_{centrifugal} = \frac{mV^2}{r} = \frac{\pi\rho d^3 V^2}{6r},$$ (11)

pushes the sphere away from the center of the arc, causing the particle to cross the fluid streamlines. Any motion of a particle relative to that of the fluid is opposed by viscous forces, resulting in two effects: first, the particle's axial velocity will very quickly become identical to the fluid's, and second, the outward motion of the particle from the centrifugal force is opposed by viscous forces acting against the particle's cross-streamline motion. The viscous force on the particle is given by Stokes' law

$$F_{viscous} = \frac{3\pi\mu Ud}{C_S}$$ (12)

with U representing the difference in velocity between the particle and the fluid. Here, specifically, it is assumed that the particle's axial velocity has matched the fluid's, so U is the particle's cross-streamline radial velocity. The balance of the centrifugal and viscous forces allows the calculation of the radial velocity,

$$U(y, z) = \frac{1}{18}\left(\frac{C_S\rho d^2 V(y, z)^2}{r\mu}\right),$$ (13)

of the particle at any point in its movement around a bend, as long as the fluid velocity V is known at that point. This equation assumes that the radius of curvature is much larger than the channel width and that the only non-diffusion force removing the particles from the streamlines is centrifugal.

D. Other effects on the particles

In curved channels or pipes, it is possible for a secondary (Dean) flow to occur. The first order Dean flow can be seen in the form of a cross-sectional flow travelling radially outwards in the channel centre, with the flow travelling back towards the radially inwards side along the top and bottom of the channel. The magnitude of the flow is determined by the dimensionless Dean number

$$De = \frac{\rho VD_H}{\mu}\sqrt{\frac{W}{2r}} = Re\sqrt{\frac{W}{2r}}.$$ (14)

The Dean flow is reported as being insignificant for De < 1, and is typically reported as beginning to occur significantly between a Dean number of 1 and 10.[21, 22] For the parameters used in the present study, the Dean number lies between 0.3 and 0.6, and so the Dean flow was not considered. In the range of $10 < De < 40$, the maximum Dean velocity was found to be $V_{Dean} = 3.9 \times 10^{-4} De^{1.63}$ m/s.[23] If this maximum Dean velocity is applied as an estimate of the possible error caused by the Dean flow, the resulting displacement due to Dean flow is 0.66 ± 0.12 μm in the range of flow conditions used in this work, which is negligible as will be seen.

The validity of the no-slip boundary condition which was used to find the flow profile in the channel is determined by the dimensionless Knudsen number, defined as the ratio of the mean free

path of fluid molecules to a characteristic physical dimension. The mean free path of air,

$$\lambda = \frac{k_B T_{air}}{\sqrt{2}\pi d_{air}^2 P},\tag{15}$$

depends on its temperature T_{air}, pressure P, and average diameter of a molecule of air d_{air}. Several regimes of flow exist depending on the Knudsen number; some literature suggests that slip flow conditions may start having discernible effects on the flow as low as Kn = 0.001.[10, 24] For a 60 μm by 100 μm rectangular channel with air at standard temperature and pressure,

$$Kn = \frac{\lambda}{d_h} \cong 9 \times 10^{-4}\tag{16}$$

is slightly below this value, suggesting that the no-slip condition is a valid assumption.

III. SIMULATIONS

A. Simulations of aerosol stream width and particle diffusion in a straight channel

The behavior of the particles in microchannels was simulated using MATLAB (v. 7.8.0 R2009a, The MathWorks Inc.). The width of the aerosol stream is determined from Eqs. (3), (4), and (6), and a number of simulated particles are placed uniformly across the aerosol stream region at the beginning of a straight channel. The Brownian motion of the particles is modeled as a random walk superimposing a step of random size in a random direction on the force-based deterministic motion of each particle. Each individual particle was followed along the channel in small time intervals; at each time interval two random numbers are generated, where α is a random number between 0 and 2π, and β is a random number chosen with a normal probability density function with mean 0 and standard deviation $\sqrt{4D\Delta t}$. From these, the particle's incremental displacement

$$\begin{aligned}\Delta x &= V(y,z)\,\Delta t,\\ \Delta y_B &= \beta\sin(\alpha),\\ \Delta z_B &= \beta\cos(\alpha),\end{aligned}\tag{17}$$

is determined, with Δx the incremental axial displacement due to the axial fluid flow (Eq. (3)), and Δy_B and Δz_B the incremental displacement in the channel width and height based on the probability distribution (Eq. (7)). Any particle that comes within one particle radius of a wall is removed.

Figure 2 shows an overview of the simulation results for two representative particle sizes (0.2 μm and 3 μm diameter) each at two different average air velocities (0.3 m/s and 0.9 m/s), corresponding to Péclet numbers between 4.4×10^7 and 4.1×10^9. The top view of the channels shows the evenly spaced particles entering at the top of the picture and traveling along the length of the channel. After each simulated particle has travelled along the full length of the channel, its final position is recorded. The final positions of all the particles for each set of conditions are compiled in the second row of pictures in Figure 2, which show the cross-sectional concentration of particles at the channel outlet; this concentration is summed height-wise to form the plots at the bottom of the figure, showing the total particle concentration across the channel width.

It can be seen that the diffusion of the particles into the sheath air regions due to the Brownian motion is more significant for smaller Péclet numbers which are associated with smaller particles (due to higher diffusion coefficients) and at lower velocities (due to longer residence times). Within each set of conditions, the diffusion of the aerosol stream into the sheath air is more pronounced at the top and bottom of the channel, as visible in the cross-sections in Figure 2. This is also an effect of residence time, since the low velocity near the wall results in a longer residence time in the channel for particles in that region, and therefore leads to a higher average distance traveled by Brownian motion.

B. Simulations of particle displacement due to centrifugal forces in a curved channel

The simulation of particle behavior in a curved channel was similar to that of a straight channel, except that at each time interval the local fluid velocity determines the balance of forces on the
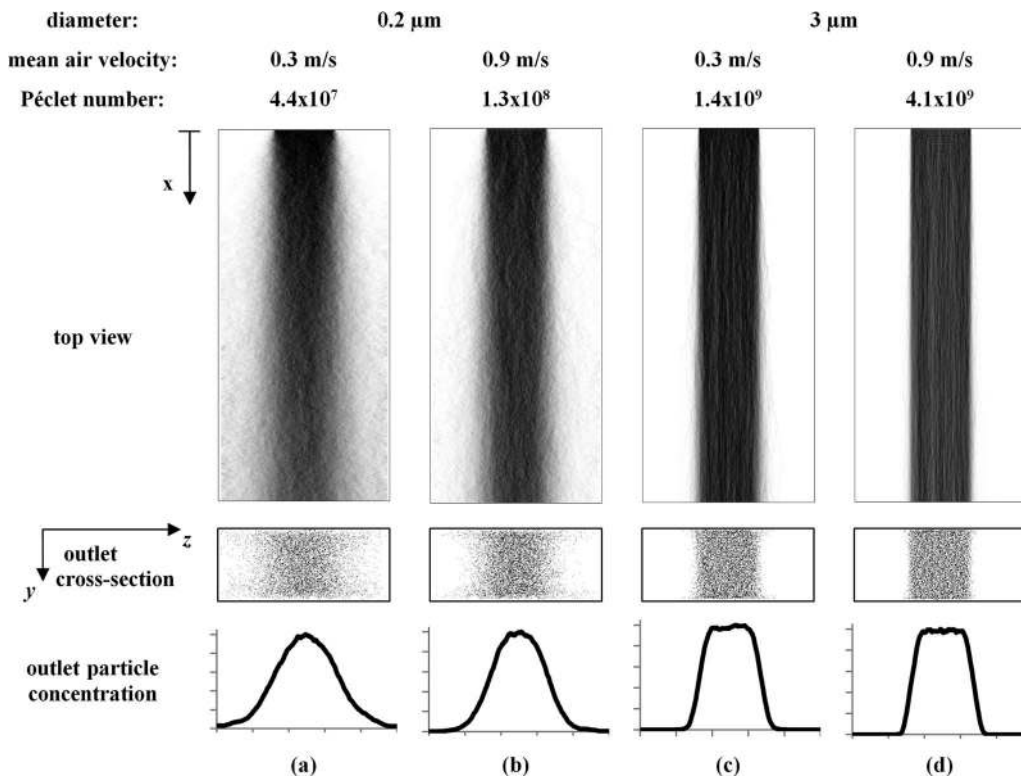
FIG. 2. MATLAB simulation of aerosol diffusion in a straight microchannel, with a top view of the whole channel, a cross-sectional view of the outlet, and a plot of concentration of particles as a function of position across the channel. Mean velocities and particle diameters are as labeled on top. The channel width is 60 μm, the height is 100 μm, and the length 4 cm; dimensions are not to scale.

particle and the resulting new particle position in the axial and radial directions was calculated before the random walk from Brownian motion was applied. The combination of the Brownian motion model with the balance of the forces (Eq. (13)) yields the change in position,

$$\Delta x = V(y, z)\, \Delta t,$$

$$\Delta y = \Delta y_B,$$

$$\Delta z = \frac{1}{18}\left(\frac{\rho d^2 V(y, z)^2}{r\mu}\right)\Delta t + \Delta z_B,$$

(18)

of the particle at each time interval. A sample simulation is shown in Figure 3, demonstrating the size-dependent displacement of 0.75 μm and 1.9 μm particles in a curved channel with a mean air velocity of 0.25 m/s (Fig. 3(a)) and 0.5 m/s (Fig. 3(b)). The separation of the particles by size is clearly seen, with more overlap in the lower-velocity simulation. It is also clear that the no-slip condition imposed at the walls limits the separation of the particle sizes, since the centrifugal force is relatively low in the low-velocity regions at the top and bottom of the channel leading to lateral dispersion of particles of the same size. However, the low-velocity regions at the side walls does help to prevent particle deposition by decreasing the radially outer velocity of the particles as they approach the outer wall of the channel.

IV. EXPERIMENTAL

To test the models, both straight and curved channels were fabricated. The straight channels were used to verify the sheath to aerosol stream flow rate ratio resulting from various inlet pressures,
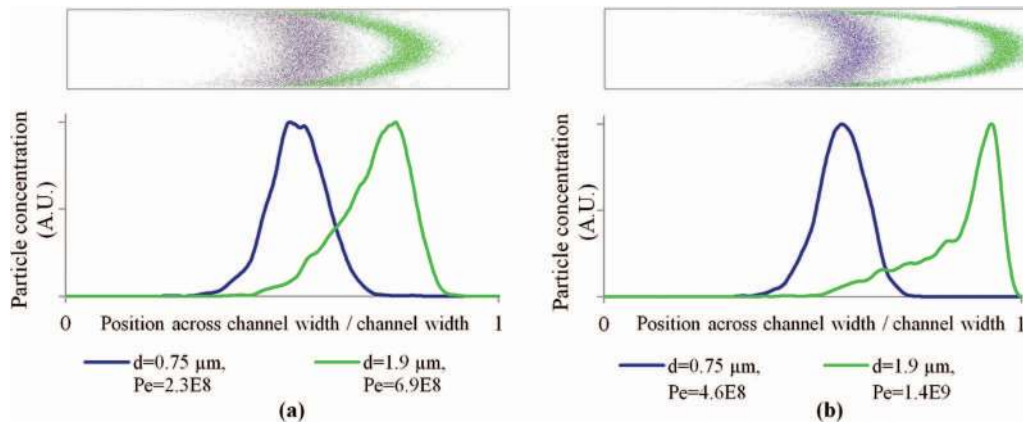
FIG. 3. MATLAB simulation results of 0.75 μm (light gray / light green online) and 1.9 μm (dark grey / dark blue online) particles undergoing separation and diffusion with average velocity (a) V_{avg} = 0.25 m/s and (b) V_{avg} = 0.5 m/s, both at a sheath to aerosol stream ratio by flow rate of 5:1. Each top picture is a cross-sectional view of the outlet with a plot of concentration of particles as a function of position across the channel for that distribution (bottom). The channel is 60 μm high and 100 μm wide. The particles travel around a 180° curve (radius of curvature 2.5 mm) and then travel a straight path after the end of the curve; the total channel length is 4 cm. Image dimensions are not to scale.

and to observe the cross-streamline diffusion of particles. Channels with a curved main section were also made to test the effect of centrifugal forces on particles of different sizes.

A. Particle generation

Polystyrene latex (PSL) microspheres were used as test particles; they are available in a wide range of highly uniform sizes and with a variety of fluorescent dyes. The different dyes (Table I) allowed for the discrimination of different particle sizes by use of optical filters on the microscope (Eclipse TE2000-U inverted microscope, Nikon Corp.).

To aerosolize the PSL microspheres, a nebulizer (Lovelace Nebulizer, In–Tox Products) was purchased and attached to a custom built drying tube. Past literature has reported a size-dependent nebulization rate for polystyrene latex microspheres in other air-jet nebulizers.[25] To calibrate our setup for this phenomenon, suspensions containing an equal number of microspheres of two different sizes were nebulized and collected. The final results were normalized so that the concentration of nebulized 0.75 μm beads equaled one and all other counts were relative to that. There was a clear correlation between larger particle diameter and decreased nebulization efficiency (Figure 4); the final numbers were used as correction factors in later analyses.

B. Experimental setup

Microchannels were fabricated with the optically transparent silicone rubber polydimethyl-siloxane (PDMS; Sylgard® 184, Dow Corning) molded from photolithography defined molds, as described in Ref. 26. The PDMS device was transected through the channel near the outlet

TABLE I. Particles and corresponding fluorescent dyes used, with the wavelength of maximum excitation (ex.) and emission (em.) for each dye.

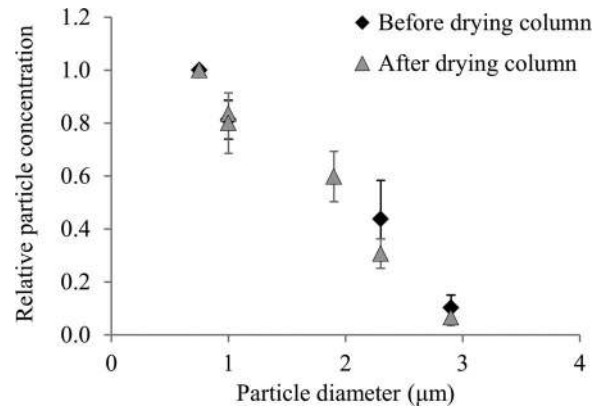| Dye	Manufacturer	Particle sizes [μm]	Ex. [nm]	Em. [nm]
yellow green (YG)	Polysciences	0.75, 2.88	441	486
suncoast yellow (SY)	Bangs Labs	2.28	540	600
orange (O)	Invitrogen	0.2	540	560
green (TG)	Thermo Scientific	1.9	468	508
red (TR)	Thermo Scientific	1.0	542	612
blue (TB)	Thermo Scientific	1.0	412	445

FIG. 4. Nebulization efficiency as a function of particle size.

to allow a piece of filter paper (MetriCEL mixed cellulose ester membrane, 0.8 μm pore, Pall Corporation) to be placed into the path of the particles which travelled along the channel during experiments.

The channels were 100 μm high, with inlets 40 μm wide and the main section 60 μm wide, with a 2.5 mm radius of curvature. At the end of the main section, the channel width expanded to 2000 μm over a length of 6 mm before the filter captured the particles; this allowed measuring the lateral position of the particles at an increased resolution. Simulations were run using COMSOL Multiphysics to confirm that the particle trajectories did not deviate noticeably from the fluid streamlines in this section.

The aerosol generation and flow control setup is shown schematically in Figure 5: the amount of air entering the microchannel from the nebulized sample was controlled by a valve connected to a bleed air line between the drying tube and the microchannel. The pressure at the split was measured and displayed in real time (LABVIEW v. 8.5; National Instruments). Pressure-controlled sheath air was provided by a MFCS-8C microfluidic pressure control system (Fluigent).

C. Method for measuring particle positions

After the particles were captured on a filter during each experiment, the filter was removed and examined on the epifluorescence microscope. The attached camera was used to take images of the
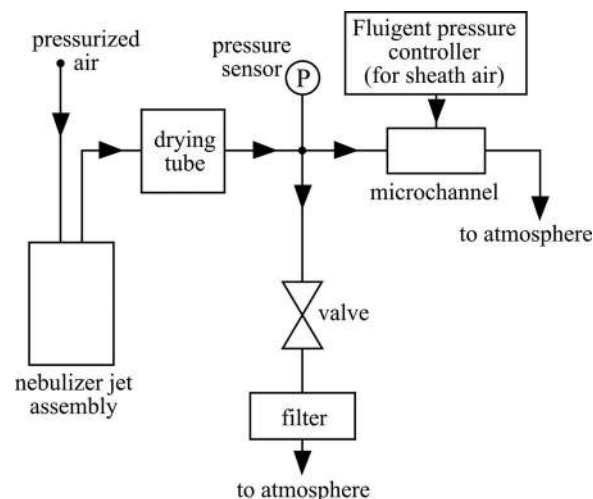

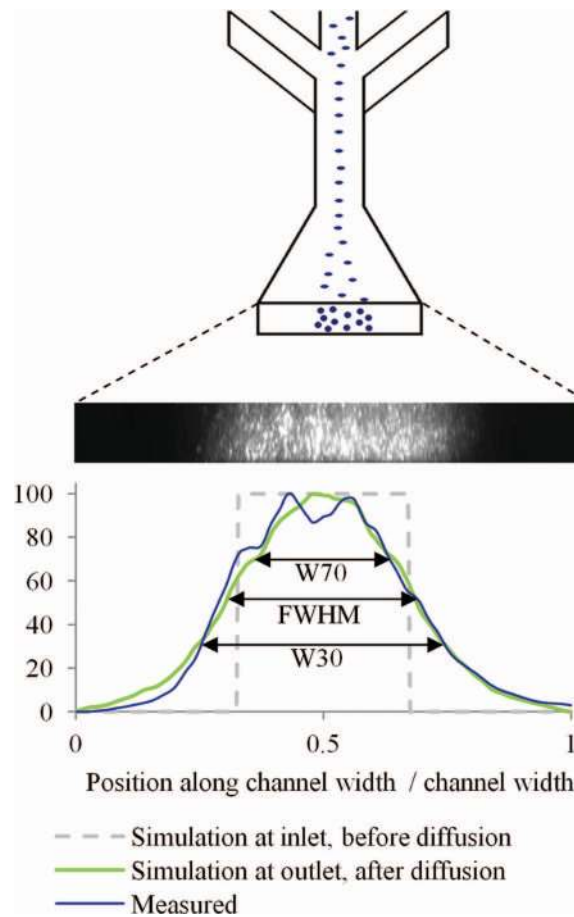FIG. 5. Schematic of the experimental setup including the nebulizer and flow control components

FIG. 6. Sample results from a straight channel experiment, with concentration plotted against position for both the experiment and a simulation run with identical conditions. The particles were 0.2 μm in diameter and the channel was 60 μm wide, 100 μm high, and 4 cm long. The total flow rate was 2.15 μL/s, with an average air velocity of 0.36 m/s, and the ratio of sheath to aerosol flow rates was 1:1. As marked here, the FWHM, W30, and W70 values are for the simulation.

particles on the filters, which were sent to a PC for capture. Images of the collected particles on the filter were imported into MATLAB (v. R2009a, The MathWorks Inc.) as matrices representing the brightness of each pixel. The image brightness was summed along each column, resulting in a plot of the intensity of the image as a function of the position along the width of the outlet as shown in Figure 2 for the simulation results. A 50-point moving average (image width = 2000 pixels) was taken to remove noise and then the values were normalized by scaling to the maximum value.

For the width and diffusion measurements, the full-width half-maximum (FWHM) width of the plot was found as a measurement of the width of the aerosol stream. Sample data from one test, with these values indicated, is shown in Figure 6. For the diffusion measurements, the difference in width of the plot at 30% ("W30") of the maximum and that of 70% ("W70") of the maximum served as a proxy for the slope of the sides, as illustrated in Figure 6.

For the curved channel experiments, two sizes of particles were used, with each size having a different color to allow them to be distinguished with the optical microscope. For each size/color, the median position of each particle size was calculated. This median position identified the point in the channel width where there was an equal amount of particles to the radially inner direction from the point as to the radially outer direction from the point. The difference in median positions for each pair of particle sizes at each velocity was found.
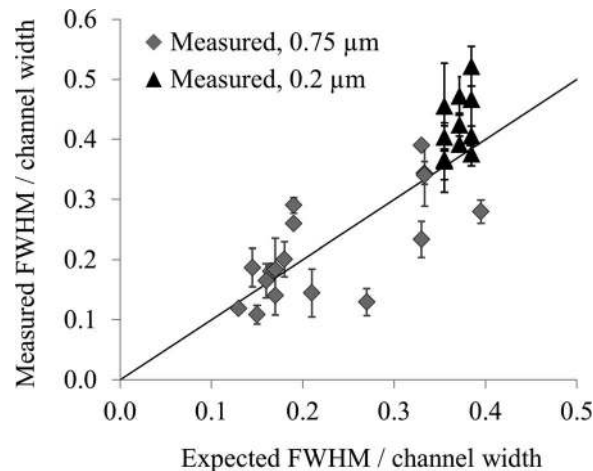
FIG. 7. Measured and expected widths in straight channel experiments. The solid black line represents the 1:1 (measured = expected) values.

V. RESULTS

A. Width of the aerosol stream in a straight microchannel

The width of the aerosol stream resulting from the flow focusing was validated in the straight channels. Tests were conducted with 0.2 μm and 0.75 μm particles. The 0.2 μm particles were tested repeatedly over a small range of sheath to aerosol flow rate ratios at a variety of total flow rates; the 0.75 μm particles were tested at a variety of ratios of sheath to aerosol flow rates and velocities chosen within the range of conditions expected to be used for the experiments.

The results showed good correlation between the width expected from the simulations and the width from the experiments (Figure 7). The average error (measured width – expected width) was 0.9% of the channel width, and the standard deviation of the measurements from the expected values was 6.6% of the channel width. The mean velocities in the main channel were between 0.3 m/s and 0.9 m/s for all but two of the tests (Reynolds number between 1.5 and 4.5), and two were at 1.8 m/s (average Re = 9).

B. Diffusion of particles in a straight microchannel

Our model for cross-stream diffusion of the particles was also validated with the straight channels. Wide streams of 0.2 μm and 1.0 μm diameter particles were each run at least three times at each of three velocities (0.7 m/s, 1 m/s, 1.4 m/s) with equal flow rates of sheath air and aerosol stream (i.e., $Q_1 = Q_2 + Q_3$), corresponding to Péclet numbers in the range 1.0×10^8 to 1.8×10^9 and average Reynolds numbers in the range 3.5 to 7 in the main separation channel.

The expected diffusion behavior of the 0.2 μm and 1.0 μm particles is summarized with the solid lines in Figure 8; the W30-W70 decreased with increasing Péclet number.

A significant factor in comparing the simulated diffusion results to the experimental ones is the number of particles used to obtain each dataset. The number of particles collected in each experiment was counted or estimated from the filter images and used for the simulations; the error bars on the simulation results in Figure 8 represent the maximum and minimum values found in the simulated results for the particle counts corresponding to the experiments done at the same velocities; they thus represent the range in which we would expect to find the corresponding experimental values. The results from both particle sizes followed the trends of the simulations; the highest velocity tests in particular (those with the highest Péclet numbers, for each particle size) were at almost exactly as predicted by the simulations, and the variation between these tests was extremely small. At lower velocities, the variability between tests increased as was predicted by the simulations.
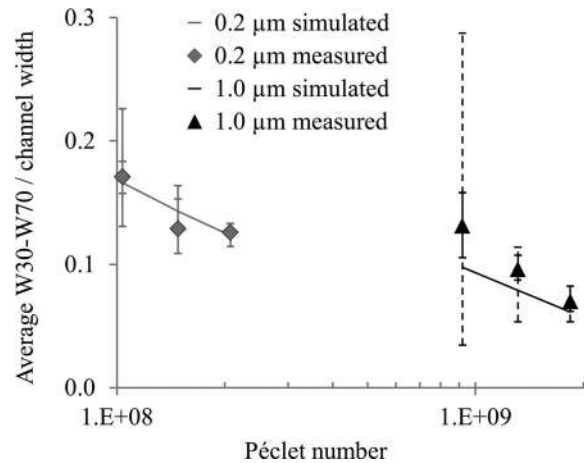
FIG. 8. Straight channel diffusion experiment results. All simulations and experiments were run at a ratio of sheath to aerosol flow rates of $(1\pm0.1){:}1$. The dashed error bars are for the simulations, and the solid error bars are for the experiments.

C. Particle displacement due to centrifugal forces in a curved microchannel

Experiments in curved channels were undertaken with test PSL particles in the range of 0.2 μm to 1.9 μm in diameter at mean channel air velocities of 0.5 m/s, 1 m/s, and 1.5 m/s, corresponding to Péclet numbers between 7.4×10^7 and 4.1×10^9 and average Reynolds numbers 2.5, 5, and 7.5 in the main separation channel. The largest of the particles were only used at the lowest velocity, as higher velocities resulted in the impaction of the particles against the radially outer wall, which results were corroborated by the simulations.

For each test, two images were taken of the filter that had been collecting particles in the microchannel outlet, using the two different microscope optical filters corresponding to fluorescence behavior of the two different particle dyes used. For some of the combinations of fluorescent dyes, minor cross-talk occurred between the two different colors; in these cases, the effects of the cross-talk were removed by using the image subtraction feature available in the image recording software. This process could be confirmed visually for each experiment, since the fluorescent emission colors of the two particles were different enough to be distinguished by eye even though they were viewed with the same optical filter. A sample for 0.2 μm particles and 0.75 μm particles is shown in Figure 9. The distinct positions of the two particle sizes on the filter can be seen; the effects of the low velocity regions near the top and bottom of the channel are also visible as particles are present near the center of the channel width at the top and bottom of both images due to lateral dispersion.

Since the absolute position of the channel outlet was not identifiable on the filter at sufficiently high accuracy, the results of these experiments are reported as relative to the position of the 0.75 μm particles at each velocity tested (Figure 10). For mixtures not containing 0.75 μm particles, the position of the larger particle size was taken as its relative position with respect to the smaller particle plus the relative position of the smaller size with respect to 0.75 μm particles under identical experimental conditions. As expected, the median particle position of larger particles with respect to 0.75 μm particles was further radially outward with increasing particle size and with increasing velocity corresponding to positive mean positions compared to the 0.75 μm particles in Fig. 10; on the other hand, smaller particles experienced less lateral displacement compared to the 0.75 μm particles corresponding to negative values in Fig. 10. Each set of experimental conditions was tested at least three times, at a ratio of sheath air to aerosol flow rates of 3:1, resulting in an aerosol stream width at the start of the main channel of approximately 10 μm.

The position of the particles by size after the curved section of the channel aligned well with the results of the simulations. The position of the 0.2 μm particles and the 1.0 μm particles relative to the 0.75 μm particles in particular were well-matched to the expected values for the three velocities tested (Figure 10). The largest particles, at 1.9 μm, showed both greater variability in the experimental results and had an average position farther from the simulated results. We speculate
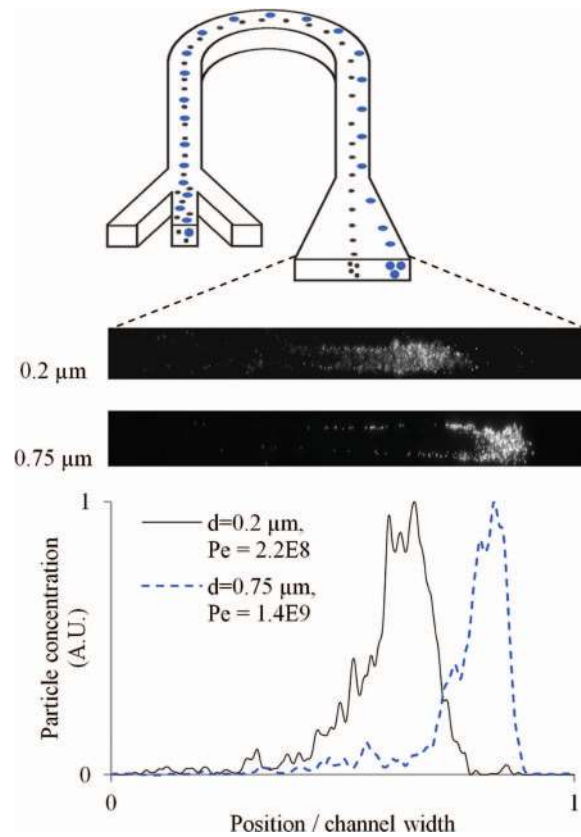
FIG. 9. Sample data for a curved channel (60 μm wide, 100 μm high, 4 cm long, 2.5 mm radius of curvature) with 0.2 μm and 0.75 μm particles. The mean channel air velocity was 1.5 m/s, and the sheath to aerosol flow rate ratio was 3:1.
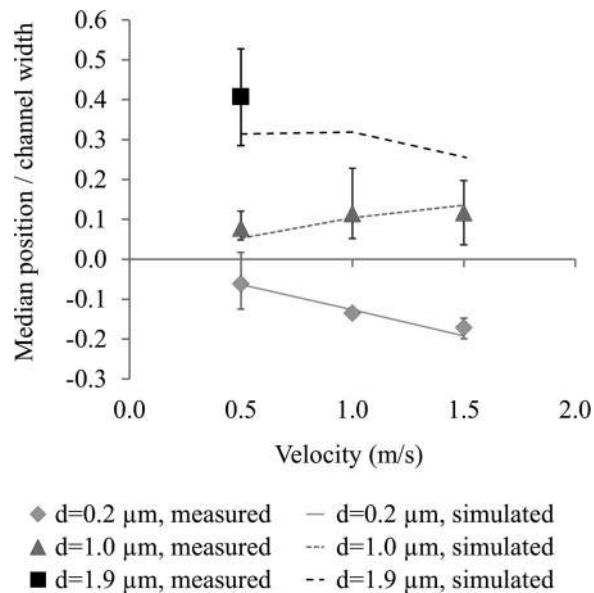

FIG. 10. Results of experiments in a single-outlet curved channel (60 μm wide, 100 μm high, 4 cm long, 2.5 mm radius of curvature), with the resulting median particle positions reported relative to the median position of 0.75 μm particles under the same conditions. The simulated results are shown with solid or dashed lines; the points represent the average value of several experiments for each set of conditions, with the error bars representing the maximum and minimum values found.

that this may be due to a similar effect as that seen in the diffusion tests: that the lower number of particles generated for larger particle sizes also increases the uncertainty in the experiments. While higher concentrations could be used to compensate for this somewhat, it was still impractical for the tests to be run long enough to produce as many particles larger than 1 μm as was easily achieved with the sub-micron particles. Despite this, the range of median particle positions measured for each set of conditions did include the value predicted by the simulations, and the average residuals (measured value – expected value) measured for the 0.5 m/s, 1 m/s, and 1.5 m/s tests were only 3.8%, 1.4%, and −3.0% of the full channel width, respectively.

VI. CONCLUSIONS

Descriptions, models, and experimental results from a microchannel-based system for the size-based displacement of aerosols have been presented. Straight channels were fabricated to validate the model of flow focusing, and to compare the measured effects of diffusion to the simulated effects for a range of Péclet numbers between 1.0×10^8 and 1.8×10^9. Curved channels were used to test the size-dependent displacement of particles in the range of 0.2 μm to 1.9 μm at a variety of velocities. The curved channel design imposes centrifugal forces on the aerosols, which travel radially outwards at a velocity dependent on their diameter and mass. The system was tested with fluorescent airborne polystyrene latex microspheres, for which the mass varies only with the diameter. The test aerosols were collected on filters placed in the path of the particles at the channel outlet; their fluorescence properties allowed them to be imaged and distinguished by size with an epifluorescence microscope. In general, the experiments showed good correlation with the simulated results. The number of particles handled in each experiment was typically fewer than was used in the simulations, resulting in greater variation in the results and accounting for some of the difference between the simulations and experiments. The good match between the simulation and experimental results suggests that the no-slip condition and particle Cunningham slip correction factor used in the initial calculations were reasonable assumptions, at least within the range of errors found in the experimental results; simulation results show that neglecting the Cunningham slip correction factor changes the expected diffusion results by between 2% and 36% for the highest and lowest Péclet number conditions used respectively.

The no-slip condition, resulting in low velocities near the wall causes both benefits and detriments to the size-dependent lateral displacement of particles traveling in a curved microchannel with respect to particle separation. The low velocity near the side walls helps to prevent the impaction of particles against the walls, since the centrifugal force pushing the particles outwards is depending on the axial velocity. However, the low velocity at the top and bottom of the channel prevents particles in those positions from being displaced laterally, leading to lateral dispersion of the particles, which would be a detriment if this approach were used in the size-separation of particles. This effect, visible in the experimental data, could be mitigated if focusing were implemented in the channel height dimension in addition to the width focusing.

To the best of the authors' knowledge, this work represents the first use of centrifugal forces to laterally displace aerosols in a curved microchannel, and is one of very few approaches that have been used for any kind of size-based separation or sorting of airborne particles in microchannels. The small footprint and potential for integration offered by microsystem fabrication technology make it a desirable avenue of pursuit for the development of small, portable particulate monitors. The results presented here confirm that this approach to size-separation is a feasible option for a future microsystem-based size-selective particulate monitor.

[1] H. Andersson and A. van den Berg, "Microfluidic devices for cellomics - a review," Sens. Actuators B **92**, 315 (2003).

[2] D. A. Ateya, J. S. Erickson, P. B. Howell, L. R. Hilliard, J. P. Golden, and F. S. Ligler, "The good, the bad, and the tiny: A review of microflow cytometry," Anal. Bioanal. Chem. **391**, 1485 (2008).

[3] K. I. Ohno, K. Tachikawa, and A. Manz, "Microfluidics: Applications for analytical purposes in chemistry and biochemistry," Electrophoresis **29**, 4443 (2008).

[4] P. S. Dittrich and A. Manz, "Lab-on-a-chip: microfluidics in drug discovery," Nat. Rev. Drug Discovery **5**, 210 (2006).

[5] S. J. Haswell and V. Skelton, "Chemical and biochemical microreactors," Trends Anal. Chem. **19**, 389 (2000).

[6] G. M. Whitesides, "The origins and the future of microfluidics," Nature (London) **442**, 368 (2006).

[7] D. Erickson and D. Li, "Integrated microfluidic devices," Anal. Chim. Acta **507**, 11 (2004).

[8] D. J. Laser and J. G. Santiago, "A review of micropumps," J Micromech. Microeng. **14**, R35 (2004).

[9] K. W. Oh and H. A. Chong, "A review of microvalves," J Micromech. Microeng. **16**, R13 (2006).

[10] M. Gad-el-Hak, "The fluid mechanics of microdevices – the Freeman Scholar lecture," J. Fluids Eng. **121**, 5 (1999).

[11] T. M. Squires and S. R. Quake, "Microfluidics: Fluid physics at the nanoliter scale," Rev. Mod. Phys. **77**, 977 (2005).

[12] B. Chua, A. S. Wexler, N. C. Tien, D. A. Niemeier, and B. A. Holmen, "Electrical mobility separation of airborne particles using integrated microfabricated corona ionizer and separator electrodes," J. Microelectromech. Syst. **18**, 4 (2009).

[13] D. Park, Y. H. Kim, C. Woo Park, J. Hwang, and Y. J. Kim, "New bio-aerosol collector using a micromachined virtual impactor," J. Aerosol Sci. **40**, 415 (2009).

[14] J. P. Black, A. Elium, R. M. White, M. G. Apte, L. A. Gundel, and R. Cambie, "MEMS-enabled miniaturized particulate matter monitor employing 1.6 GHz aluminum nitride thin-film bulk acoustic wave resonator (FBAR) and thermophoretic precipitator," in *IEEE Ultrasonics Symposium*, edited by M. P. Yuhas (IEEE, New York, 2007), p. 476.

[15] A. Hajjam, J. C. Wilson, A. Rahafrooz, and S. Pourkamali, "Fabrication and characterization of thermally actuated micromechanical resonators for airborne particle mass sensing: II. Device fabrication and characterization," J. Micromech Microeng. **20**, 125019 (2010).

[16] Committee on the Medical Effects of Air Pollutants, *Cardiovascular Disease and Air Pollution* (UK Department of Health, 2006).

[17] C. A. Pope, R. T. Burnett, M. J. Thun, E. E. Calle, D. Krewski, K. Ito, and G. D. Thursten, "Lung cancer, cardiopulmonary mortality, and long-term exposure to fine particulate air pollution," J. Am. Med Assoc. **287**, 1132 (2002).

[18] M. L. Bell and D. L. Davis, "Reassessment of the lethal London fog of 1952: Novel indicators of acute and chronic consequences of acute exposure to air pollution," Environ. Health Perspect. **109**, 389 (2001).

[19] F. M. White, *Viscous Fluid Flow* (McGraw-Hill, New York, 2005).

[20] E. Cunningham, "On the velocity of steady fall of spherical particles through fluid medium," Proc. R. Soc. London, Ser. A **83**, 357 (1910).

[21] D. Di Carlo, D. Irimia, R. G. Tompkins, and M. Toner, "Continuous inertial focusing, ordering, and separation of particles in microchannels," Proc. Natl. Acad. Sci. U.S.A. **104**, 18892 (2007).

[22] S. Kim and S. J. Lee, "Measurement of Dean flow in a curved micro-tube using micro digital holographic particle tracking velocimetry," Exp. Fluids **46**, 255 (2009).

[23] S. Ookawara, R. Higashi, D. Street, and K. Ogawa, "Feasibility study on concentration of slurry and classification of contained particles by microchannel," Chem. Eng. J. **101**, 171 (2004).

[24] A. A. Rostami, A. S. Mujumdar, and N. Saniei, "Flow and heat transfer for gas flowing in microchannels: a review," Heat Mass Transfer **38**, 359 (2002).

[25] O. N. M. Mc Callion, K. M. G. Taylor, M. Thomas, and A. J. Taylor, "Nebulisation of monodisperse latex sphere suspensions in air jet and ultrasonic nebulisers," Int. J. Pharm. **133**, 203 (1996).

[26] A. Schaap, W. Chu, and B. Stoeber, "Continuous size-separation of airborne particles in a microchannel for aerosol monitoring," IEEE Sens. J. **11**, 2790 (2011).